Catalysis Letters (2023) 153:824–835
https://doi.org/10.1007/s10562-022-04016-0

ZIF-8@ZIF-67 Derived Co/NPHC Catalysts for Efficient and Selective Hydrogenation of Nitroarenes

Jianbo Zhao[1] · Weichuang Yang[1] · Haifeng Yuan[1] · Xiaomeng Li[1] · Wanzhen Bing[1] · Lifeng Han[2] · Konglin Wu[3]

Received: 19 February 2022 / Accepted: 13 April 2022 / Published online: 30 April 2022

Abstract

Constructing nitrogen-doped porous hollow carbon with loading of non-precious metal for highly efficient hydrogenation of nitroarenes is desirable but challenging. Herein we report a facile self-sacrificing template strategy to prepare Co embedded in nitrogen-doped porous hollow carbon (Co/NPHC) from pyrolysis of well-designed core–shell ZIF-8@ZIF-67. The pyrolysis of ZIF-8@ZIF-67 at 900 °C endowed as-resultant Co/NPHC-900 with high specific surface area, hollow structure and hierarchical mesopore, favoring the dispersion of Co species and then generating abundant Co-N_x active sites, also promoting mass transport of substrates and products. As a result, the Co/NPHC-900 catalyst showed excellent activity and extraordinary selectivity in the hydrogenation of nitrobenzene, which far surpassed Co/NPC-900 and ZnCo/NPC-900 catalysts derived from sole ZIF-67 and ZnCo-BMZIF, respectively. It also had a broad substrate scope and good reusability. Furthermore, characterization and control experiments showed that Co single atoms should be catalytic active sites rather than Co nanoparticles for Co/NPHC-900. Our work provides a good candidate for the replacement of precious metal catalysts for selective hydrogenations as well as contributes to the rational design of high-performance single-atom catalysts.

Graphical abstract

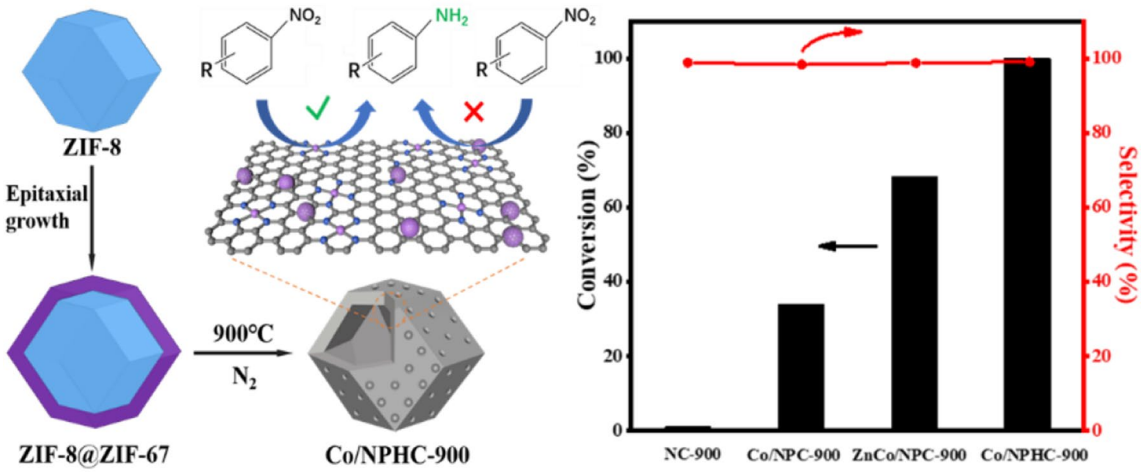

Keywords ZIF-8@ZIF-67-Co · NPHC · Hydrogenation · Nitroarene

1 Introduction

As pivotal organic raw materials and intermediates, aromatic amines have been widely used in the fields of dyes, medicines and pesticides [1, 2]. Aromatic amines are

✉ Jianbo Zhao
zhaojianbo@zzuli.edu.cn

✉ Konglin Wu
klwuchem@ahut.edu.cn

Extended author information available on the last page of the article

mainly manufactured from corresponding nitroarenes with stoichiometric reducing agents such as Fe, Zn, Sn, and NaSH in chemical industry [3]. These non-catalytic processes unavoidably produced a large number of undesirable waste and then led to environmental problems. Therefore catalytic hydrogenation of nitroarenes with molecular hydrogen has become the preferred choice due to environmental friendliness and high efficiency [4–6]. Noble metal catalysts are known to show high catalytic property for this kind of reaction, but most of them cannot meet the dual requirements of activity and selectivity. The widely used Pt group metals with high intrinsic activity usually sustain low selectivity in the hydrogenation of nitroarenes containing other reductive groups [5, 6]. To improve the selectivity, these catalysts are modified by poisoning with well-chosen additives or alloying with other metals but at the expense of activity. Au catalysts with extraordinary selectivity delivered the low intrinsic activity, thereby requiring a high reaction temperature and/or high pressure of H_2. [7–9] Recently, some noble metal single atom catalysts have been reported to show high activity and selectivity for the hydrogenation of nitroarenes even under mild conditions [4, 10]. Nevertheless, the scarcity and high cost of noble metal catalysts tremendously restricted the large-scale application in chemical industry [7–16]. It is highly desired to explore high-performance non-noble metal catalyst for hydrogenation of nitroarenes.

In this spirit, many earth-abundant metal catalysts (i.e., Fe, Co, and Ni) have been developed successfully [17–25]. Raney-Ni catalysts were extensively used in many hydrogenation reactions, but they required special handling and also suffered from dehalogenation phenomenon in the hydrogenation of halogen-substituted nitroarenes [17, 18]. Till now, Co supported on carbon-based catalysts would be preferred because of good activity and excellent selectivity in the hydrogenation of nitroarenes, especially substituted nitroarenes. Beller et al. for the first time used stable and nanoscale Co_3O_4 surrounded by N-doped carbon layer for the hydrogenation of nitroarenes with a wide scope under 5 MPa H_2 at 110 °C [20]. Afterwards Co-Co_3O_4@NCNTs was report to be a promising catalyst for selective nitroarene hydrogenation under 3 MPa H_2 at 110 °C, whereas Co@C displayed excellent catalytic performance at more than 120 °C [21, 22]. Although significant achievements over Co-based metal catalysts in recent years, most catalysts still required high pressure of H_2 (> 2 MPa) and/or high reaction temperature (> 100 °C) due to low intrinsic activity. To increase the activity, a useful template strategy to enlarge the dispersion of Co active sites and mass transport of substrates and products was widely employed, but it possessed some drawbacks such as the relatively complicated preparation process and the high cost of specific reagents. Developing Co-based catalysts with a facile and efficient strategy is still challenging.

As a kind of representative metal–organic frameworks, zeolitic imidazolate frameworks (ZIFs) have been excellent platforms to fabricate non-noble metal catalysts due to controllable composition, adjustable structure, abundant carbon and nitrogen [26–29]. For instance, ZIF-67 derived Co-based catalysts have exhibited fascinating potential for hydrogenation of nitroarenes to corresponding anilines [30–32]. However, the derivatives from single ZIF-67 had certain disadvantages of the low specific surface area and poor porosity, which obstructed the dispersion of active sites, accessibility of active sites and mass transport, thus resulting in a low activity [33]. Constructing hierarchical porous hollow carbon materials with loading of Co from well-designed MOF precursors, facilitating the dispersion of active sites and transport and diffusion of substrates, would significantly increase the catalytic property.

Bearing the above consideration in mind, herein a facile self-sacrificing template strategy was reported to obtain Co embedded in nitrogen-doped hierarchical porous hollow carbon (Co/NPHC) from pyrolysis of well-designed core–shell ZIF-8@ZIF-67. ZIF-67 was used as carbon, nitrogen and cobalt precursor, whereas ZIF-8 acted as additional carbon and nitrogen precursor as well as the template to generate the hollow structure due to Zn vaporization at high temperature. The as-resultant Co/NPHC-900 catalyst at pyrolysis temperature of 900 °C possessed the abundant Co-N_x active sites with a hollow and hierarchical nanopore structure. Therefore the Co/NPHC-900 catalyst showed excellent activity and extraordinary selectivity in the hydrogenation of nitrobenzene, which far surpassed Co/NPC-900 and ZnCo/NPC-900 catalysts, respectively. It also had a broad substrate scope and good reusability. Characterization and control experiments showed that Co single atoms instead of Co nanoparticles should be catalytic active sites for Co/NPHC-900 catalysts. To our knowledge, it is the first report on a MOF-derived hollow nanostructure for nitroarene hydrogenation with excellent activity and selectivity. These made Co/NPHC-900 promising for the replacement of precious metal catalysts for nitroarene hydrogenation.

2 Experimental

2.1 Materials

Cobalt nitrate ($Co(NO_3)_2{\cdot}6H_2O$, 98.5%) and zinc nitrate ($Zn(NO_3)_2{\cdot}6H_2O$, 99%) were purchased from Tianjin Kermel Chemical Reagent Co. Ltd. 2-methylimidazole (2-MeIM, 98%), nitrobenzene (AR, 99%), 4-nitrochlorobenzene (AR, 99.5%), 4-nitrostyrene (AR, 97 wt %), p-nitrobenzaldehyde (AR, 97 wt %), 3,5-dimethylnitrobenzene (AR, 98 wt %), p-nitrosotoluene (AR, 99%) and aniline (AR, 99.5%) were

bought from Shanghai Macklin Biochemical Co. Ltd. Methanol (AR, ≥ 98.5%) and ethanol (AR, ≥ 99.7%) were obtained from Tianjin Zhiyuan Chemical Reagent Co. Ltd.

2.2 Preparation of ZIF-8

ZIF-8 was synthesized using $Zn(NO_3)_2{\cdot}6H_2O$ and 2-methylimidazole according to the reported previous research with some modifications [34]. 0.94 g of $Zn(NO_3)_2{\cdot}6H_2O$ was first dissolved in the mixture composed of 20 mL of methanol and 20 mL deionized water and stirred 10 min. 20 mL of methanol containing 2.0 g 2-methylimidazole was added to the above solution and stirred 2 h at room temperature. The precipitation was collected by centrifugation, washed with methanol several times, and dried in vacuum at 60 ℃ for overnight.

2.3 Preparation of ZIF-67 and ZnCo-BMZIF

1.45 g of $Co(NO_3)_2{\cdot}6H_2O$ and 1.54 g of 2-methylimidazole were dissolved in 50 mL methanol and stirred for 10 min, respectively. 2-methylimidazole solution was dropped into the $Co(NO_3)_2$ solution and stirred at room temperature for 24 h. The purple precipitate was centrifuged, washed with methanol for 3 times, and dried in vacuum at 60 ℃ for 12 h. 50 mL methanol containing 0.97 g of $Co(NO_3)_2{\cdot}6H_2O$ and 0.5 g of $Zn(NO_3)_2{\cdot}6H_2O$ was used instead of the Co solution above to obtain ZnCo-BMZIF by the similar preparation process.

2.4 Preparation of ZIF-8@ZIF-67

250 mg of ZIF-8 was dispersed 50 mL methanol and sonicated for 15 min. The 50 mL methanol containing 1.46 g of $Co(NO_3)_2{\cdot}6H_2O$ was first added into ZIF-8 solution and stirred for 30 min, and then the 50 mL methanol containing 1.54 g of 2-methylimidazole was dropped into the above mixed solution and stirred for 24 h at room temperature. The precipitation was collected by centrifugation, washed with methanol several times, and dried in vacuum at 60 ℃ for 12 h.

2.5 Preparation of Co@NPHC-T

The as-prepared ZIF-8@ZIF-67 were heated to the designated temperature with a heating rate of 2 °C min^{-1} under N_2 atmosphere, and maintained for 1 h to obtain Co/NPHC-T. T represented the pyrolysis temperature. Other Co-based materials were prepared from their corresponding precursors by the similar treatment process.

2.6 Characterizations of Catalysts

Their phase structures of samples were tested by X-ray diffraction (XRD) patterns using a Bruker D8 diffractometer system with Cu Kα1 incident radiation (λ = 1.5406 Å, 20°-80°). The surface morphologies of samples were measured using field emission scanning electron microscopy (FESEM, JSM-7001F), transmission electron microscopy (TEM, JEM-2100) and aberration-corrected high-angle annular-dark-field scanning transmission electron microscopy (AC-HADDF-STEM, NEOARM). The specific surface area and pore distribution of samples were characterized via Brunner-Emmet-Teller (BET, Belsorp-mini II) measurements. The chemical compositions and states of samples were tested by the X-ray photoelectron spectrometer (XPS, Thermo Fisher Scientific). The metal loadings were tested by atomic absorption spectrophotometry (AAS).

2.7 Property of Catalysts

Selective hydrogenation of nitroarenes was performed in a batch reactor. Typically, 0.01 g of catalysts, 4.0 mL of ethanol and 0.5 mmol of nitroarenes were added to the autoclave. Then the reactor was purged with H_2 for 4 times and pressured to 1.0 MPa H_2, followed by being stirred under reaction conditions. After the reaction ended, the analysis of reaction mixture was carried out by GC and GC–MS with o-xylene as the internal standard. The used catalyst was obtained by centrifugation and dried for the next run.

3 Results and Discussion

3.1 Catalysts Characterizations

The synthetic procedure of Co/NPHC-900 catalysts was presented in Scheme 1. Briefly, ZIF-8 was first prepared according to the reported research [34]. And then core–shell ZIF-8@ZIF-67 was obtained through growth of ZIF-67 on the surface of ZIF-8 due to their homologous crystal structures [35, 36]. Figure 1A and Fig. 1S showed that ZIF-8@ZIF-67 and ZIF-8 possessed identical rhombic dodecahedral structures, respectively, but the former had a little larger diameter (about 500 nm) compared to ZIF-8 (a diameter of around 400 nm), which was caused by epitaxial growth. EDS elemental mapping images from Fig. 1B showed that Zn and Co were mainly distributed over the center and outside of the sample, indicating the generation of ZIF-8@ZIF-67 core–shell nanostructures with the shell thickness of approximately 50 nm. ZIF-67 and CoZn-BMZIF were also synthesized for comparison and their SEM images were provided in Fig. 2S. Figure 3S demonstrated that these samples exhibited the same diffraction patterns, consistent with

Scheme 1 The synthetic procedure of Co/NPHC-900 catalysts

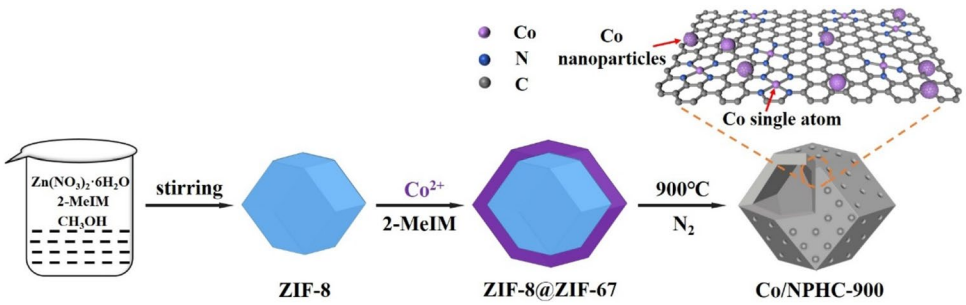

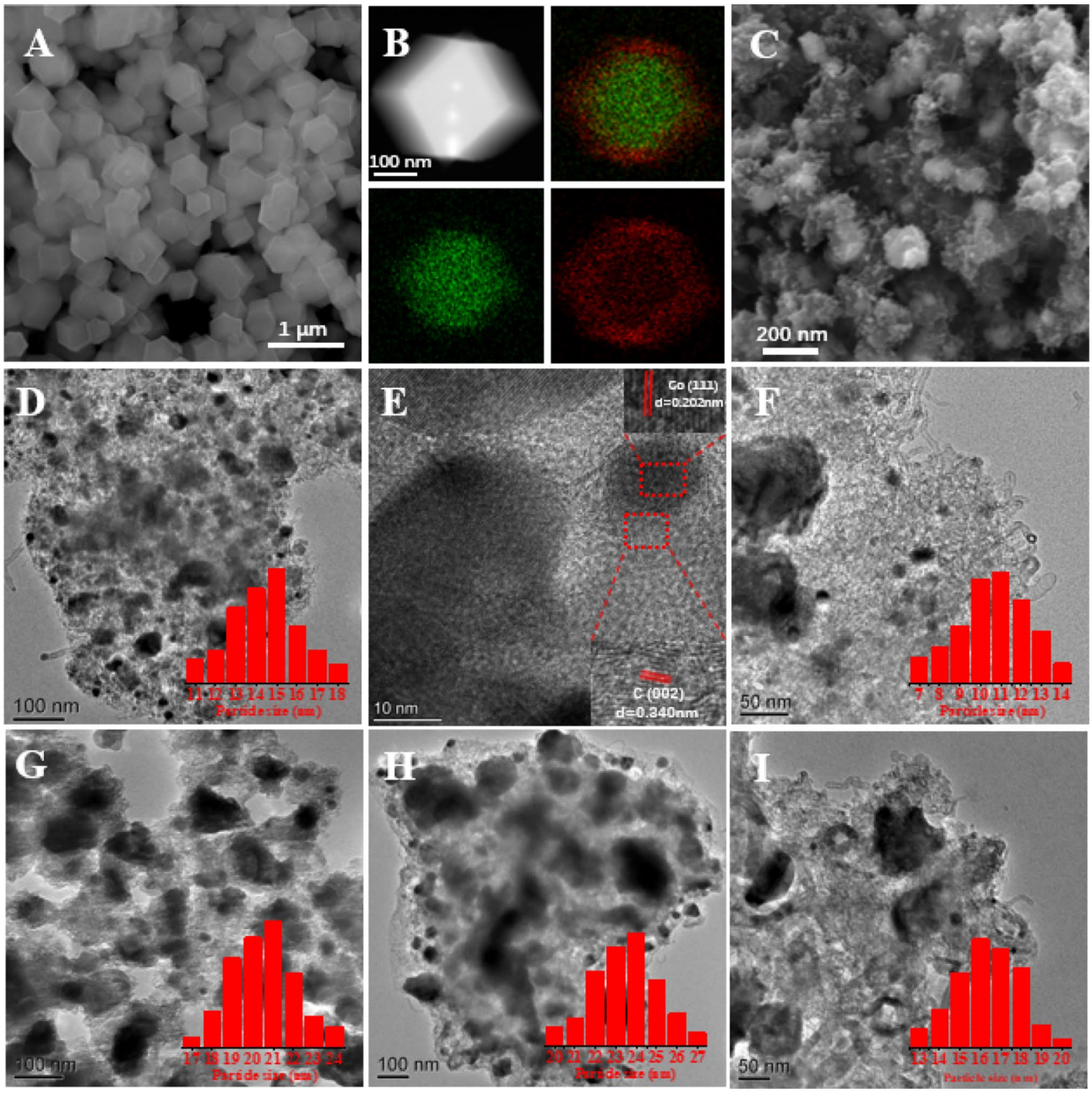

Fig. 1 **A**, **B** SEM and HAADF-STEM elemental mapping images of ZIF-8@ZIF-67; **C** SEM images of Co/NPHC-900; **D**, **E** TEM and HRTEM images of Co/NPHC-900, insets show lattice fringe image of Co@NPHC-900; **F**–**I** TEM images of Co@NPHC-800, Co@NPHC-1000, Co@NPC-900 and CoZn@NPC-900

those of previous reported ZIF-8 and ZIF-67 [37]. These confirmed the successful formation of core–shell nanostructured ZIF-8@ZIF-67.

After the annealing of ZIF-8@ZIF-67 under N_2, nitrogen-doped hollow carbon framework wrapped by many carbon nanotubes with the loading of Co (Co/NPHC-900) were observed in Fig. 1C. The formation of carbon nanotubes was mainly related to the catalytic behavior of Co nanoparticles derived from ZIF-8@ZIF-67, and then the evaporation of Zn accelerated this process [38, 39]. Figure 1D showed that Co nanoparticles with an average size of 14.3 nm generated due to the reduction of reductive gases from the pyrolysis of organic ligands and coated by nitrogen-doped carbon layer or confined in carbon nanotubes. The HRTEM image in Fig. 1E revealed that the lattice distance of Co nanoparticles is around 0.202 nm, which was ascribed to the (111) plane of metallic Co. It was also observed that Co nanoparticles were encapsulated in few-layered carbon with a

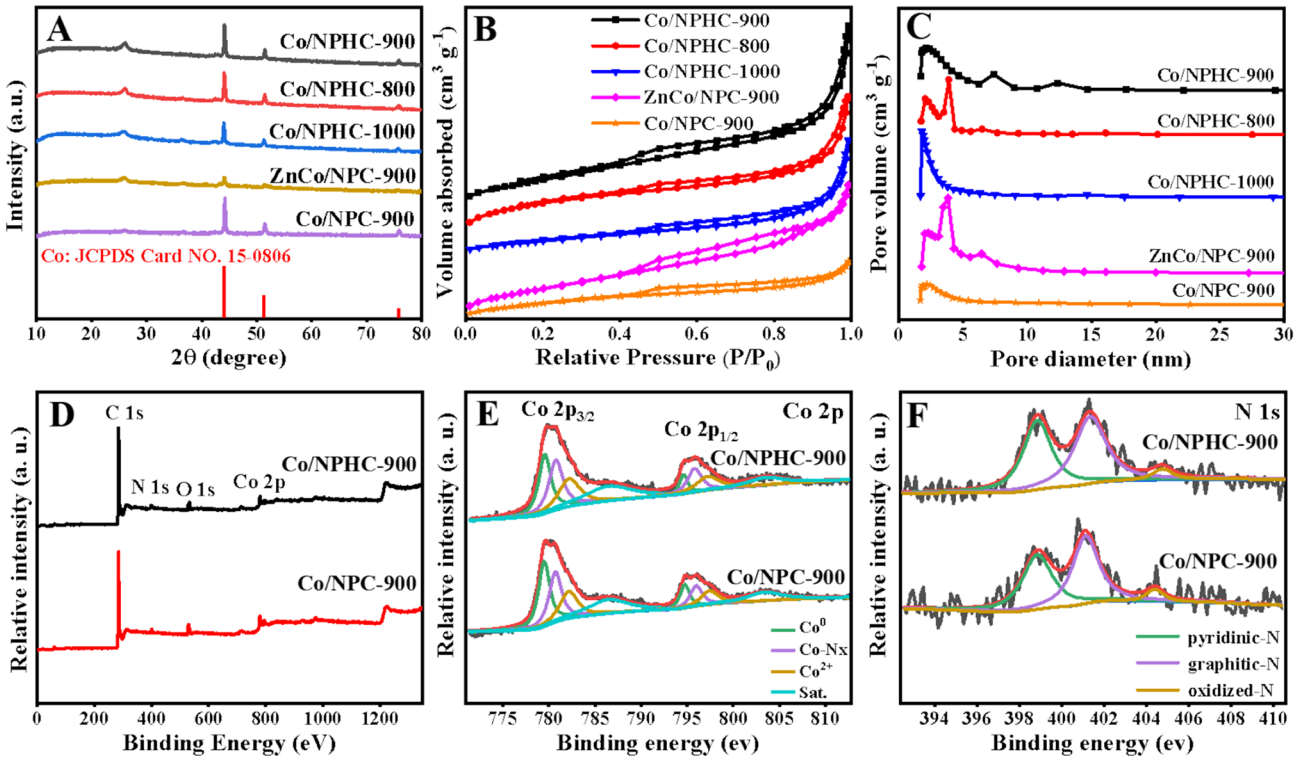

Fig. 2 **A** XRD patterns of samples; **B** N_2 sorption isotherms, **C** porous size distribution plots of samples; **D** XPS survey spectra, **E**, **F** high-resolution Co 2p, N 1 s spectra of Co@NPHC-900 and Co@NPC-900, respectively

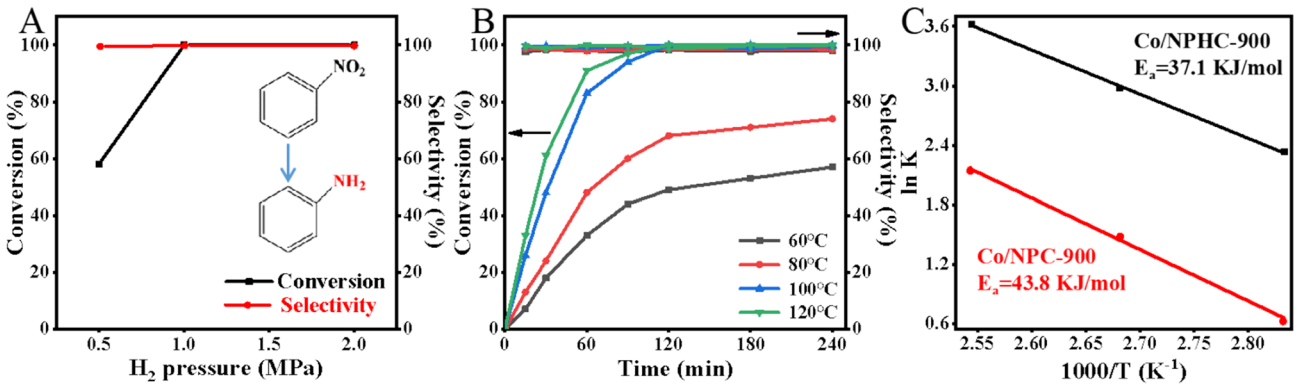

Fig. 3 **A** Effect of H_2 pressure on catalytic performance of Co/NPHC-900 (temperature,100 °C); **B** reaction temperature effect (H_2 pressure, 1.0 MPa H_2); **C** Arrhenius plots for nitrobenzene hydrogenation over Co/NPHC-900 and Co/NPC-900 catalysts. Other reaction conditions: nitrobenzene, 0.5 mmol; ethanol, 4 mL; catalyst, 0.01 g; stirring speed, 600 rpm

lattice distance of 0.340 nm, assigned to the (002) plane of graphitic carbon. Typical TEM images of samples from the carbonization of ZIF-8@ZIF-67 at different temperatures were listed in Fig. 1F and G. It can be found that the size of Co nanoparticles gradually increased with increasing pyrolysis temperature. They obviously tended to aggregate when it reached 1000 °C, which resulted in the agglomeration of metal species. For comparison, the corresponding SEM and TEM of Co/NPC-900 and CoZn/NPC-900, acquired from the thermal treatment of plain ZIF-67 and ZnCo-BMZIF, respectively, were provided in Fig. 4S, Fig. 1H–I. It showed that the evaporation of Zn from ZIF-8@ZIF-67 not only generated the hollow structure at high pyrolysis temperature, but also partly avoided the agglomeration of Co nanoparticles, in accordance with the previous reports [38–40].

XRD patterns of Co/NPHC-800, Co/NPHC-900, Co/NPHC-1000, Co/NPC-900 and CoZn/NPC-900 were listed in Fig. 2A. Three peaks at around 44.4, 51.5 and 76.2° are seen, which belonged to the (111), (200) and (220) facets of face-centered cubic Co (PDF No. 15–0806). No Co oxide and carbide were found, suggesting that divalent Co had been completely reduced to metallic Co at high pyrolysis temperature. The peak located at 25.8° was ascribed to the (002) plane of graphitic carbon. These results agreed well with TEM results above. The porous properties of samples, closely associated with catalytic activity, were investigated by nitrogen adsorption/desorption (Fig. 2B and Table 1S). These samples showed a type-IV isotherm with a H1 hysteresis, suggesting the existence of the mesoporous structure [41, 42]. Co/NPHC-900, Co/NPHC-800 and Co/NPHC-1000 had large surface areas of 404.0, 255.9 and 327.6 m^2/g

Table 1 Catalytic hydrogenation of nitrobenzene over as-prepared Co catalysts

Entry	Catalysts	Co content / wt% [a]	Conv /% [b]	Sel /% [b]	TOF /h^{-1} [c]
1	blank	–	–	–	
2	NC-900	–	0.4	> 99	
3	Co/NPHC-800	26.5	86.7	98.3	9.8
4	Co/NPHC-900	29.5	100	> 99	11.2
5	Co/NPHC-1000	30.2	71.2	98.7	3.1
6	Co/NPC-900	34.3	34.8	98.4	2.4
7	ZnCo/NPC-900	32.8	68.2	97.6	4.3
8[d]	Co/NPHC-900	29.5	92	> 99	
9[e]	Co/NPHC-900-AL	16.0	100	> 99	
10[f]	Co/NPHC-900-AL-KSCN	16.0	16.7	> 99	
11[g]	Co NPs/NPC-900	16.0	18.5	> 99	

Reaction conditions: nitrobenzene, 0.5 mmol; ethanol, 4 mL; catalyst, 0.01 g; 100 °C; 1 MPa H_2; stirring speed 600 rpm

[a]The weigh amount of Co was test by AAS

[b]The conversion of nitrobenzene and selectivity towards aniline were determined by GC

[c]TOF (h^{-1}) was also calculated from moles of converted nitrobenzene per mole of Co per hour with the results at 15 min

[d]The results of the four use

[e]The Co/NPHC-900-AL catalyst was obtained by treating Co/NPHC-900 in 2 mol/L HCl aqueous solution under stirring for 10 h at room temperature

[f]KSCN of 20 equiv to Co were added

[g]Co NPs/NPC was prepared from the incipient wetness impregnation method with $Co(NO_3)_2{\cdot}6H_2O$ and NPC-900 as Co precursor and support, respectively

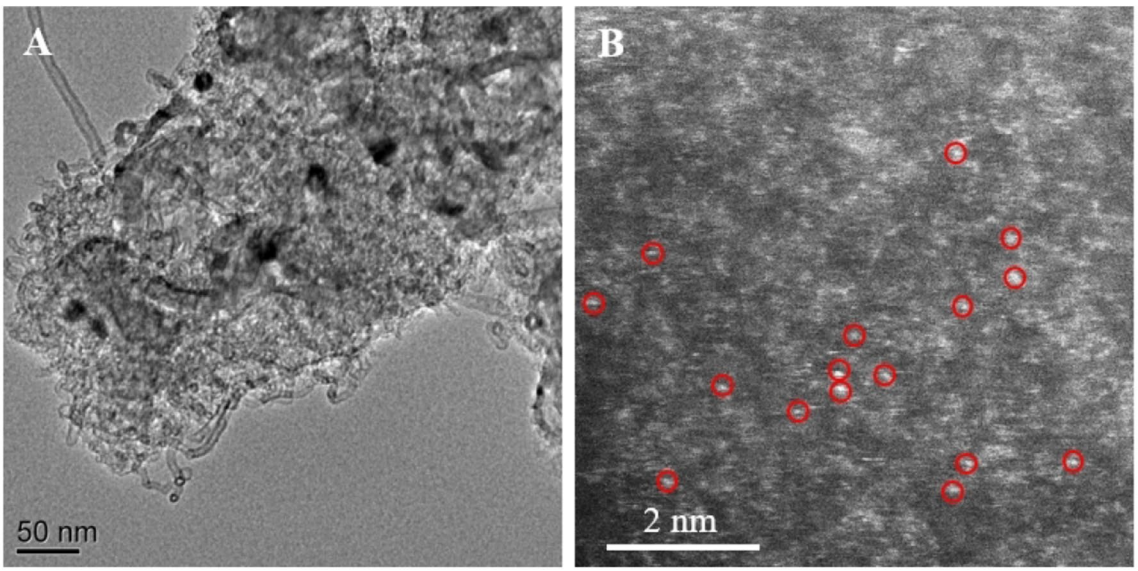

Fig. 4 **A** TEM and **B** AC-HADDF-STEM images of Co@NPHC-900-AL

and pore volumes of 0.62, 0.40 and 0.51 cm^3/g, respectively. The pore size distribution plots of them indicated that the mean pore sizes were mostly in the range of 2–5 nm (Fig. 2C). Besides, the Co/NPHC-900 also possessed two kinds of mesopore with porous size of about 7.5 nm and 12.5 nm. As comparison, Co/NPC-900 from sole ZIF-67 gave a low specific surface area of 142.2 m^2/g and pore volume of 0.22 cm^3/g, which also displayed worse porous property than ZnCo/NPC-900 with a BET surface area of 301.9 m^2/g and pore volume of 0.47 cm^3/g, derived from ZnCo-BMZIF. The different porous structures demonstrated the pivotal role of core–shell ZIF-8@ZIF-67 architecture as precursor. So the Co/NPHC-900 possessed large specific surface area, hollow structure and hierarchical nanopore, in favour of anchoring and exposing the catalytic sites (e.g., Co-N_x) and promoting mass transport of substrates, respectively, which finally contributed to the catalytic hydrogenation activity.

The elemental composition and chemical states of samples were presented by XPS. The full XPS spectra showed the signal of C, N, O and Co, indicating the successful doping of Co and N atoms into the carbon network by the pyrolysis process (Fig. 2D). High-resolution N 1 s spectra from Fig. 2E exhibited three peaks positioned at about 398.9, 401.4 and 404.7 eV, which were assigned to pyridinic-N, graphitic-N and oxidized-N, respectively [40, 43]. It was reported that nitrogen species exercised a considerable influence over catalytic performance. The presence of nitrogen species not only facilitated the dispersion of Co, but also generated Co-N_x species during the pyrolysis process because of the interaction between Co and N, which was considered to be catalytic active sites [32, 40, 44, 45]. Noted that the peak located at 398.9 eV was also partially originated from a contribution of nitrogen bound to the metal (Co-N_x) due to the similarity in chemical environment of pyridinic N and Co-N_x. [45] In any case, Co/NPHC-900 had more surface content of N species than Co/NPC-900 (Table 2S), related to ZIF-8@ZIF-67 as precursor, which was advantageous for catalysis. Likewise, the Co 2p spectra was deconvolved. Four peaks located at binding energies of 778.8, 780.2, 781.6 and 786.1 eV in Fig. 2F were ascribed to Co^0, Co-N_x, Co^{2+} and satellite peak, respectively [32, 43]. The generation of Co^{2+} species was probably associated with the surface oxidation of exposed Co nanoparticles that were not encapsulated with graphitic layers [46]. The Co/NPHC-900 catalyst possessed 35.5% content of Co-N_x species, higher than Co/NPC-900 catalyst with 32.6%, which would be conductive to catalytic activity enhancement.

Table 2 Substrate scope of nitroarene hydrogenation over Co/NPHC-900 catalysts

Entry	Substrate	Time(h)	Conv./% [a]	Sel./% [a]
1	Nitrobenzene	2	100	> 99
2	p-Nitrotoluene	4	98.6	> 99
3	4-Nitrostyrene	8	94.4	98.3
4	4-Nitrochlorobenzene	6	97.4	> 99
5	p-Nitrobenzaldehyde	8	98.5	97.1
6	3,5-Dimethylnitrotoluene	7	96.3	98.5

Reaction conditions: nitrobenzene and its derivatives, 0.5 mmol; ethanol, 4 mL; catalyst, 0.01 g; 100 °C;1 MPa H_2; stirring speed 600 rpm

[a]The conversion of nitrobenzene and its derivatives and selectivity towards aromatic amines were determined by GC and GC–MS

3.2 Catalytic Properties

As an important chemical reaction in both academic and industry, hydrogenation of nitrobenzene to aniline was chosen to assess the catalytic properties of as-prepared catalysts and the results were listed in Table 1. No activity for nitrobenzene hydrogenation was found without catalyst (Table 1, entry 1). It showed this reaction only proceeded in the presence of catalyst. Similarly, almost no conversion of nitrobenzene was obtained over NC-900 catalysts from pyrolysis of ZIF-8 at 900 °C, indicating that only nitrogen-doped carbon cannot catalyze the reaction (Table 1, entry 2). Under the identical reaction conditions, the Co/NPHC-800 derived from ZIF-8@ZIF-67 showed significantly enhanced property with 86.7% conversion of nitrobenzene and 98.3% selectivity towards aniline, proving that Co species (e.g., Co-N_x) was catalytic active sites for nitrobenzene hydrogenation (Table 1, entry 3). And then the Co/NPHC-900 catalyst delivered the complete conversion and more than 99% selectivity (Table 1, entry 4). To further show the intrinsic activity of catalysts, the nitrobenzene conversion was restricted to less than 30% by using the results at reaction time of 15 min, and the turn-over frequency (TOF, h^{-1}) was calculated from on the basis of the molar amount of Co. It was seen that the Co/NPHC-900 catalyst gave the TOF of 11.2 h^{-1}, exhibiting higher activity than Co/NPHC-800 and Co/NPHC-1000 catalysts (Table 1, entries 3–5). Moreover, the catalytic performance of Co/NPHC-900 catalyst was superior or comparable to other reported Co-based catalysts (Table 3S). According to characterization results above, the Co/NPHC-800 and Co/NPHC-900 catalysts had comparable specific surface area and particle size distribution, so the effects of them on catalytic property were excluded. The hollow nanostructured framework formed for Co/NPHC-900 because of Zn evaporation at 900 °C, which probably resulted in the enhanced activity. The matrix structure was seriously broken (e.g., the breakage of C-N and Co-N_x) and the active sites agglomeration were also severe at 1000 °C,

so the Co/NPHC-1000 catalyst displayed the inferior catalytic activity.

To further clarity the advantages of ZIF-8@ZIF-67 as precursor, the Co/NPC-900 catalyst was prepared from pyrolysis of sole ZIF-67 and used as catalyst for hydrogenation of nitrobenzene. It delivered the TOF of 2.4 h^{-1}, which is almost one fifth of that of Co/NPHC-900, showing a very low catalytic activity (Table 1, entry 6). As the characterization results above, the Co/NPHC-900 catalyst had high specific surface area and rich surface N content relative to Co/NPC-900, thus generating the more Co-N_x species and then boosting catalytic performance. Besides, its hollow structure and hierarchical nanopore promoted mass transport of reactants and products, enhancing the nitrobenzene conversion. The ZnCo/NPC-900 catalyst was also obtained from ZnCo-BMZIF as comparison, exhibiting low conversion with maintaining the similar selectivity (Table 1, entry 7). All of these results confirmed the unique role of ZIF-8@ZIF-67 as precursor.

The effects of H_2 pressure, reaction temperature and time were studied. The influence of H_2 pressure on hydrogenation of nitrobenzene was carried out under the temperature of 100 °C and reaction time of 2 h. As seen from Fig. 3A, the conversion of nitrobenzene increased with the increasing pressure of H_2. It was related to the enhanced dissolution of H_2 molecules in the solvent derived from higher H_2 pressure. Around 100% nitrobenzene conversion and more than 99% selectivity towards aniline were accomplished when H_2 pressure remained 1.0 MPa. The effect of reaction temperature on the nitrobenzene hydrogenation was investigated under 1 MPa H_2 (Fig. 3B). As expected, increasing the reaction temperature led to higher conversion of nitrobenzene when the reaction proceeded for the same time. For example, the conversion of nitrobenzene increased from 47 to 71% and 100% with reaction temperature increasing from 60 °C to 80 °C and 100 °C at the reaction time of 2 h. Furthermore, the Co/NPHC-900 and Co/NPC-900 catalysts gave the apparent activation energies of 37.1 and 43.8 kJ/mol with their pre-exponential factors of 4.5×10^6 h^{-1} and 2.6×10^6 h^{-1}, respectively, which were derived from the Arrhenius plots obtained in the temperature range of 80–120 °C (Fig. 3C). Both the lower activation energy and higher pre-exponential factor of Co/NPHC-900 led to higher catalytic activity. Noted that more than 99% selectivity towards aniline was achieved, indicating that the selectivity was independent on reaction conditions used in our work. The excellent selectivity towards aniline was probably ascribed to preferential adsorption of the nitro group on Co-N_x sites, which was reported by Li's group [30]. An increase in reaction time resulted in an enhanced nitrobenzene conversion and complete conversion was obtained at 100 °C after 2 h (Fig. 3B). Besides, the Co/NPHC-900 catalyst gave good recyclability, which delivered about 92% nitrobenzene conversion and unchanged selectivity when it used for four consecutive runs (Table 1, entry 8). The XRD (Fig. 5S) and TEM (Fig. 6S) of Co/NPHC-900 after recycling showed little change, confirmed the good stability. Therefore it was a highly active, selective and stable catalyst for hydrogenation of nitrobenzene.

To identify the catalytic active sites is of great importance for illuminating the catalytic mechanism and designing high-performance catalysts. So far, a great number of heterogeneous Co catalysts showed high performance for hydrogenation of nitroarenes, whereas the nature of catalytic sites was still at the center of intense debate. Beller's group attributed the high activity of nanoscale Co_3O_4 surrounded by N-doped carbon layer to the Co oxide-N moiety [20]. It was communicated that H_2 could access the surface of Co nanoparticles by small cracks of thin carbon layers for the Co@C catalyst and so accessible Co nanoparticles accounted for catalytic activity [21]. Some researchers claimed that nitrogen-doped graphene or carbon nitride tuned by underlying Co or Ni nanoparticles served as active sites for H_2. [17, 22] Both Co nanoparticles and atomically dispersed Co species were also reported to be active sites for Co@NC-800 derived from pristine ZIF-67 [31]. Recently, Co single atoms anchored different nitrogen-doped carbon have been confirmed to be efficient catalysts for selective hydrogenation of nitro compounds [47–49]. With regard to our catalyst, what were the real catalytic sites? To address this problem, control experiments were performed. First, the Co/NPHC-900 catalyst were treated in 2 mol/L HCl aqueous solution under stirring for 10 h at room temperature. The Co/NPHC-900-AL catalyst was tested by a series of characterization techniques. Figure 4A showed that many voids were observed for the as-prepared etched-Co catalyst (Co/NPHC-900-AL), indicating that many accessible Co particles were removed after acid treatment. It was confirmed by the reduced Co content of Co/NPHC-900-AL, which was 16.0 wt% tested by AAS. As seen from XRD results (Fig. 7S), the peak intensity of face-centered cubic Co for Co/NPHC-900-AL decreased, which was associated with the removal of accessible Co particles from acid treatment. It was in accordance with the AAS and TEM test. The results from N_2 adsorption/desorption (Fig. 8S and Table 1S) showed that no obvious change about the porous properties of Co/NPHC-900-AL was observed. XPS (Fig. 9S) characterizations confirmed the presence of Co, C and N elements for Co/NPHC-900-AL, however, its content of Co-N_x (34.8%) was lower than that of Co/NPHC-900, which was probably related to the loss of Co particles. Noted that some Co particles still existed in the Co/NPHC-900-AL catalyst, indicating that Co nanoparticles were totally encapsulated by multiple graphitic carbon shells. These Co were inaccessible even to H_2, thereby making little contribution to catalytic activity [31, 50]. It was worth nothing that the Co/NPHC-900-AL showed no

decrease in conversion and selectivity in the nitrobenzene hydrogenation (Table 1, entry 9). These results suggested that Co nanoparticles including accessible Co nanoparticles and Co nanoparticles fully encapsulated by carbon layer are unlikely to be active sites.

To obtain further information on the active sites, the poison test on the Co/NPHC-900-AL catalysts was carried out. As a well-known poison reagent for metal single atom catalysts, KSCN was used to explore the poison effect [51, 52]. When KSCN (20 equivalent relative to the molar of Co) was introduced into the reaction, the nitrobenzene conversion significantly decreased from 100% to 16.7% over the Co/NPHC-900-AL catalyst (Table 1, entry 10). This phenomenon was be explicated by the strong interaction between SCN^- and Co single atoms, suggesting that Co single atoms provided catalytic sites for nitrobenzene hydrogenation. Meanwhile, AC-HADDF-STEM (Fig. 4B) showed that many bright dots (marked by red circles) were found in Co nanoparticle-free regions, indicating the presence of Co single atoms. Transitional metal atoms such as Co and Fe formed during pyrolysis process were reactive towards heteroatoms such as N to generate atomically dispersed metal-N_x species embedded in the carbon matrix, and these as-formed metal-N_x species were very stable and exhibited good acid resistance property [46–49]. Combined with TEM and HRTEM characterizations of Co/NPHC-900, there was indeed the coexistence of Co nanoparticles and Co–N-C sites in Co/NPHC-900. Due to strong ferromagnetism of Co nanoparticles, herein the HADDF-AC-STEM characterization of Co/NPHC-900-AL was only provided. According to reported researches, however, the coexistence phenomenon of Co nanoparticles and Co–N-C sites could be found for Co/NPC-900 [31, 48]. As comparison, the Co NPs/NPC-900 catalyst was prepared from the incipient wetness impregnation method with $Co(NO_3)_2{\cdot}6H_2O$ and NPC-900 as Co precursor and support, respectively. [49] It showed the inferior activity, only affording 18.5% conversion of nitrobenzene under identical reaction conditions (Table 1, entry 11). According to control experiments and characterization results, Co single atoms existing in the form of Co-N_x species for Co/NPHC-900 were the main catalytic active sites rather than accessible Co nanoparticles or Co nanoparticles encapsulated by thick carbon layer.

The N-doping type in carbon had an important influence on catalytic property of M-N_x-C [53–55]. To clarify their effect, the N species were required to be precisely regulated. Wang et al. reported that the major N species as pyrrolic-N and pyridinic-N respectively were obtained through compounding with different metal oxides, and the as-resultant pyrrolic-N coordinated Cu single atom catalyst displayed much higher activity for transfer hydrogenation of quinoline [54]. Chen et al. found that the FeN_4/graphitic N atomic interface facilitated the synergistic adsorption of H_2O and CO_2 and then promoted CO_2 electrocatalytic reduction, constructed by preferentially eliminating undesired pyrrolic-N and pyridinic-N using a hydrogen-pyrolysis strategy [55]. Both Co/NPHC-900 and Co/NPC-900 had two major kinds of N species (pyridinic-N and graphitic-N) (Table 2**S**). Due to the commonly random doping behaviors of N species in N-doped carbon, they can not be differentiated from N1s XPS. So the effect of N species for our catalysts on hydrogenation of nitrobenzene and their cooperation was not elucidated. It was worthy of further study in future. Besides, the catalytic recycling of Co/NPHC-900-AL was evaluated in the hydrogenation of nitrobenzene. No noticeable decrease in activity was observed without modifying the selectivity to aniline when it reused for four runs (Fig. 10S), the conversion changing from 100 to 90%. It show that the Co/NPHC-900-AL catalyst possessed good reusability.

Finally, the scope of nitroarene hydrogenation catalyzed by the Co/NPHC-900 catalyst were investigated (Table 2). The transformation of different nitroarenes to aromatic amines was accomplished over Co/NPHC-900 catalysts with high conversion and selectivity. For substituted nitrobenzens, it took longer reaction time to achieve almost full conversion. Noted that Co/NPHC-900 catalysts selectively hydrogenated the nitro group instead of other competitive groups such as -Cl, -C = C and -CHO, which was very important for hydrogenation of nitroarenes with co-existence of other reductive groups. These results showed that the Co/NPHC-900 catalyst was highly active and chemoselective for hydrogenation of different nitro compounds.

4 Conclusions

We report a self-sacrificing template strategy to achieve Co embedded in nitrogen-doped hierarchical porous hollow-structured carbon (Co/NPHC-900) from pyrolysis of well-designed core–shell ZIF-8@ZIF-67. The as-resultant Co/NPHC-900 catalyst exhibited excellent activity and extraordinary selectivity in the hydrogenation of nitrobenzene, which far surpassed Co/NPC-900 and ZnCo/NPC-900 catalysts, respectively. The enhanced propertied were related to abundant Co-N_x active sites and fast mass transport of substrates and products, which were resulted from its hollow structure, hierarchical nanopore and high specific area. It also had a broad substrate scope and good reusability. Characterization and control experiments showed that Co single atoms should be catalytic active sites rather than Co nanoparticles for Co/NPHC-900. These made Co/NPHC-900 catalysts promising for the replacement of precious metal catalysts for selective hydrogenations.

Supplementary Information The online version contains supplementary material available at https://doi.org/10.1007/s10562-022-04016-0.

Acknowledgements The work was financially supported by the National Natural Science Foundation of China (21576248) and Key scientific research projects of colleges and universities of Henan Province (21A150057).

Funding Key scientific research projects of colleges and universities of Henan Province, 21A150057, National Natural Science Foundation of China, 21576248

Declarations

Conflict of interest The authors declare that they have no conflict of interest.

References

1. Zhao JB, Jin RC (2018) Heterogeneous catalysis by gold and gold-based bimetal nanoclusters. Nano Today 18:86–102
2. Blaser H, Steiner H, Studer M (2009) Selective catalytic hydrogenation of functionalized nitroarenes: an update. ChemCatChem 1:210–221
3. Baumeister P, Blaser H, Scherrer W, Guisnet M, Barrault J, Bouchoule C, Duprez D, Pérot G, Maurel R, Montassier C (1991) Chemoselective hydrogenation of aromatic chloronitro compounds with amidine modified nickel catalysts. Stud Surf Sci Catal 59:321–328
4. Wei HS, Liu XY, Wang AQ, Zhang LL, Qiao BT, Yang XF, Huang YQ, Miao S, Liu JY, Zhang T (2014) FeO_x-supported platinum single-atom and pseudo-single-atom catalysts for chemoselective hydrogenation of functionalized nitroarenes. Nat Commun 5:5634
5. Song JJ, Huang ZF, Pan L, Li K, Zhang XW, Wang L, Zou JJ (2018) Review on selective hydrogenation of nitroarene by catalytic, photocatalytic and electrocatalytic reactions. Appl Catal B 227:386–408
6. Zhao JB, Ge LM, Yuan HF, Liu YF, Gui YH, Zhang BD, Zhou LM, Fang SM (2019) Heterogeneous gold catalysts for selective hydrogenation: from nanoparticles to atomically precise nanoclusters. Nanoscale 11:11429–11436
7. Corma A, Serna P (2006) Chemoselective hydrogenation of nitro compounds with supported gold catalysts. Science 313:332–334
8. Zhao JB, Li Q, Zhuang SL, Song YB, Morris DJ, Zhou M, Wu ZK, Zhang P, Jin RC (2018) Reversible control of chemoselectivity in $Au_{38}(SR)_{24}$ nanocluster-catalyzed transfer hydrogenation of nitrobenzaldehyde derivatives. J Phys Chem Lett 9:7173–7179
9. He L, Wang LC, Sun H, Ni J, Cao Y, He HY, Fan KN (2009) Efficient and selective room-temperature gold-catalyzed reduction of nitro compounds with CO and H_2O as the hydrogen source. Angew Chem Int Ed 48:9538–9541
10. Lin L, Yao S, Gao R, Liang X, Yu Q, Deng Y, Liu J, Peng M, Jiang Z, Li S, Li YW, Wen XW, Zhou W, Ma D (2019) A highly CO-tolerant atomically dispersed Pt catalyst for chemoselective hydrogenation. Nat Nanotechnol 14:354–361
11. Lu CS, Zhu QW, Zhang XJ, Ji HK, Zhou YB, Wang H, Liu QQ, Nie JJ, Han WF, Li XN (2019) Decoration of Pd nanoparticles with N and S doped carbon quantum dots as a robust catalyst for the chemoselective hydrogenation reaction. ACS Sustain Chem Eng 7:8542–8553
12. Guo M, Li H, Ren YQ, Ren XM, Yang QH, Li C (2018) Improving catalytic hydrogenation performance of Pd nanoparticles by electronic modulation using phosphine ligands. ACS Catal 8:6476–6485
13. Berguerand C, Yarulin A, Cárdenas-Lizana F, Wärnå J, Sulman E, Murzin DY, Kiwi-Minsker L (2015) Chemoselective liquid phase hydrogenation of 3-nitrostyrene over Pt nanoparticles: synergy with ZnO support. Ind Eng Chem Res 54:8659–8669
14. Zhang QS, Bu JH, Wang JD, Sun CY, Zhao DY, Sheng GZ, Xie XW, Sun M, Yu L (2020) Highly efficient hydrogenation of nitrobenzene to aniline over Pt/CeO_2 catalysts: the shape effect of the support and key role of additional Ce^{3+} sites. ACS Catal 10:10350–10363
15. Qin RX, Zhou LY, Liu PX, Gong Y, Liu KL, Xu CF, Zhao Y, Gu L, Fu G, Zheng NF (2020) Alkali ions secure hydrides for catalytic hydrogenation. Nat Catal 3:703–709
16. Deng X, Qin B, Liu RZ, Qin XT, Dai WL, Wu GJ, Guan NJ, Ma D, Li LD (2021) Zeolite-Encaged Isolated Platinum Ions Enable Heterolytic Dihydrogen Activation and Selective Hydrogenations. J Am Chem Soc 143:20898–20906
17. Fu T, Wang M, Cai WM, Cui YM, Gao F, Peng LM, Chen W, Ding WP (2014) Acid resistant catalysis without use of noble metals: carbon nitride with underlying nickel. ACS Catal 4:2536–2543
18. Huang L, Lv Y, Liu SH, Cui HS, Zhao ZY, Zhao H, Liu PL, Xiong W, Hao F, Luo HA (2020) Non-noble metal Ni nanoparticles supported on highly dispersed TiO_2-modified activated carbon as an efficient and recyclable catalyst for the hydrogenation of halogenated aromatic nitro compounds under mild conditions. Ind Eng Chem Res 59:1422–1435
19. Jagadeesh RV, Surkus A, Junge H, Pohl M, Radnik J, Rabeah J, Huan H, Schünemann V, Brückner A, Beller M (2013) Nanoscale Fe_2O_3-based catalysts for selective hydrogenation of nitroarenes to anilines. Science 342:1073–1076
20. Westerhaus FA, Jagadeesh RV, Wienhöfer G, Pohl M, Radnik J, Surkus A, Rabeah J, Junge K, Junge H, Nielsen M, Brückner A, Beller M (2013) Heterogenized cobalt oxide catalysts for nitroarene reduction by pyrolysis of molecularly defined complexes. Nat Chem 5:537–543
21. Liu LC, Concepción P, Corma A (2016) Non-noble metal catalysts for hydrogenation: a facile method for preparing Co nanoparticles covered with thin layered carbon. J Catal 340:1–9
22. Wei ZZ, Wang J, Mao SJ, Su DF, Jin HY, Wang YH, Xu F, Li HR, Wang Y (2015) In situ-generated Co^0-Co_3O_4/N-doped carbon nanotubes hybrids as efficient and chemoselective catalysts for hydrogenation of nitroarenes. ACS Catal 5:4783–4789
23. Formenti D, Ferretti F, Scharnagl FK, Beller M (2019) Reduction of nitro compounds using 3d-non-noble metal catalysts. Chem Rev 119:2611–2680
24. Cao YL, Liu KK, Wu C, Zhang HP, Zhang QY (2020) In situ-formed cobalt embedded into N-doped carbon as highly efficient and selective catalysts for the hydrogenation of halogenated nitrobenzenes under mildconditions. Appl Catal A Gen 592:117434
25. Shen ZY, Hong LR, Zheng BS, Wang GY, Zhang BB, Wang ZX, Zhan FY, Shen SH, Yun RR (2021) Highly efficient and chemoselective hydrogenation of nitro compounds into amines by nitrogen-doped porous carbon-supported Co/Ni bimetallic nanoparticles. Inorg Chem 60:16834–16839
26. Wang HF, Chen LY, Pang H, Kaskel S, Xu Q (2020) MOF-derived electrocatalysts for oxygen reduction, oxygen evolution and hydrogen evolution reactions. Chem Soc Rev 49:1414–1448
27. Lu XF, Fang YJ, Luan DY, Lou XW (2021) Metal-organic frameworks derived functional materials for electrochemical energy storage and conversion: a mini review. Nano Lett 21:1555–1565
28. Xiong Y, Dong JC, Huang ZQ, Xin PY, Chen WX, Wang Y, Li Z, Jin Z, Xing W, Zhuang ZB, Ye JY, Wei X, Cao R, Gu L, Sun SG, Zhuang L, Chen XQ, Yang H, Chen C, Peng Q, Chang CR, Wang DS, Li YD (2020) Single-atom Rh/N-doped carbon electrocatalyst for formic acid oxidation. Nat Nanotechnol 15:390–397
29. Shen K, Chen XD, Chen JY, Li YW (2016) Development of MOF-derived carbon-based nanomaterials for efficient catalysis. ACS Catal 6:5887–5903

30. Wang X, Li YW (2016) Chemoselective hydrogenation of functionalized nitroarenes using MOF-derived Co-based catalysts. J Mol Catal A 420:56–65
31. Sun XH, Olivos-Suarez AI, Oar-Arteta L, Rozhko E, Osadchii D, Bavykina A, Kapteijn F, Gascon J (2017) Metal-organic framework mediated cobalt/nitrogen-doped carbon hybrids as efficient and chemoselective catalysts for the hydrogenation of nitroarenes. ChemCatChem 9:1854–1862
32. Dai YY, Li XQ, Wang LK, Xu XS (2021) Highly efficient hydrogenation reduction of aromatic nitro compounds using MOF derivative Co-N/C catalyst. New J Chem 45:22908–22914
33. Wang H, Yin FX, Li GR, Chen BH, Wang ZQ (2014) Preparation, Characterization and Bifunctional Catalytic Properties of MOF (Fe/Co) Catalyst for Oxygen Reduction/Evolution Reactions in Alkaline Electrolyte. Int J Hydrogen Energy 39:16179–16186
34. Liédana N, Galve A, Rubio C, Téllez C, Coronas J (2012) CAF@ ZIF-8: one-step encapsulation of caffeine in MOF. ACS Appl Mater Interfaces 4:5016–5021
35. Park KS, Ni Z, Côte AP, Choi JY, Huang RD, Uribe-Romo FJ, Chae HK, O'Keeffe M, Yaghi OM, (2006) Exceptional chemical and thermal stability of zeolitic imidazolate frameworks. Natl Acad Sci U S A 103:10186–10191
36. Banerjee R, Phan A, Wang B, Knobler C, Furukawa H, O'Keeffe M, Yaghi OM (2008) High-throughput synthesis of zeolitic imidazolate frameworks and application to CO_2 capture. Science 319:939–943
37. Tang J, Salunkhe RR, Liu J, Torad NL, Imura M, Furukawa S, Yamauchi Y (2015) Thermal conversion of core-shell metal-organic frameworks: a new method for selectively functionalized nanoporous hybrid carbon. J Am Chem Soc 137:1572–1580
38. Pan Y, Sun KA, Liu SJ, Cao X, Wu KL, Cheong WC, Chen Z, Wang Y, Li Y, Liu YQ, Wang DS, Peng Q, Chen C, Li YD (2018) Core-shell ZIF-8@ZIF-67-Derived CoP nanoparticle-embedded N-doped carbon nanotube hollow polyhedron for efficient overall water splitting. J Am Chem Soc 140:2610–2618
39. Yun RR, Hong LR, Ma WJ, Zhang RY, Zhan FY, Duan JG, Zheng BS, Wang SN (2020) Co Nanoparticles encapsulated in nitrogen doped carbon tubes for efficient hydrogenation of quinoline under mild conditions. ChemCatChem 12:129–134
40. Xiong W, Zhou SS, Wang LP, Liu Y, Hao F, Liu PL, Luo HA (2020) ZIF-derived Co-based catalysts for efficient hydrogenation of aromatic compounds: the study of the Co-N_x active sites. Ind Eng Chem Res 59:22473–22484
41. Zhao JB, Yuan HF, Guang Y, Liu YF, Qin XM, Zheng C, Weng-Chon C, Zhou LM, Fang SM (2022) AuPt bimetallic nanoalloys supported on SBA-15: A superior catalyst for quinoline selective hydrogenation in water. Nano Res 15:1796–1802
42. Zhao JB, Yuan HF, Qin XM, Tian K, Liu YF, Wei CZ, Zhang ZQ, Zhou LM, Fang SM (2020) Au nanoparticles confined in SBA-15 as a highly efficient and stable catalyst for hydrogenation of quinoline to 1,2,3,4-tetrahydroquinoline. Catal Lett 150:2841–2849
43. Chen SY, Bi FF, Xiang K, Zhang Y, Hao PP, Li MH, Zhao B, Guo XF (2019) Reactive template-derived CoFe/N-doped carbon nanosheets as highly efficient electrocatalysts toward oxygen reduction, oxygen evolution, and hydrogen evolution. ACS Sustain Chem Eng 7:15278–15288
44. Gong WB, Lin Y, Chen C, Al-Mamun M, Lu HS, Wang GZ, Zhang HM, Zhao HJ (2019) Nitrogen-doped carbon nanotube confined Co-Nx sites for selective hydrogenation of biomass-derived compounds. Adv Mater 31:180834
45. He WH, Jiang CH, Wang JB, Lu LH (2014) High-rate oxygen electroreduction over graphitic-N species exposed on 3D hierarchically porous nitrogen-doped carbons. Angew Chem Int Ed 53:9503–9507
46. Zhang EH, Xie Y, Ci SQ, Jia JC, Cai PW, Yi LC, Wen ZH (2016) Multifunctional High-Activity and Robust Electrocatalyst Derived from Metal-Organic Frameworks. J Mater Chem A 4:17288–17298
47. Han YH, Wang ZY, Xu RR, Zhang W, Chen WX, Zheng LR, Zhang J, Luo J, Wu KL, Zhu YQ, Chen C, Peng Q, Liu Q, Hu P, Wang DS, Li YD (2018) Ordered porous nitrogen-doped carbon matrix with atomically dispersed cobalt sites as an efficient catalyst for dehydrogenation and transfer hydrogenation of N-heterocycles. Angew Chem Int Ed 57:11262–11266
48. Li MH, Chen SY, Jiang QK, Chen QL, Wang X, Yan Y, Liu J, Lv CC, Ding WP, Guo XF (2021) Origin of the activity of Co-N-C catalysts for chemoselective hydrogenation of nitroarenes. ACS Catal 11:3026–3039
49. Wang HJ, Wang Y, Li YF, Lan XC, Ali B, Wang TF (2020) Highly efficient hydrogenation of nitroarenes by N-doped carbon supported cobalt single-atom catalyst in ethanol/water mixed solvent. ACS Appl Mater Interfaces 12:34021–34031
50. Li JL, Liu GL, Long XD, Gao G, Wu J, Li FW (2017) Different active sites in a bifunctional Co@N-doped graphene shells based catalyst for the oxidative dehydrogenation and hydrogenation reactions. J Catal 355:53–62
51. Luo HH, Wang LY, Shang SS, Li GS, Lv Y, Gao S, Dai W (2020) Cobalt nanoparticles catalyzed widely applicable successive C-C bond cleavage in alcohols to access esters. Angew Chem Int Ed 59:19268–19274
52. Liang HW, Brüller S, Dong RH, Zhang J, Feng XL, Müllen K (2015) Molecular metal-N_x centres in porous carbon for electrocatalytic hydrogen evolution. Nat Commun 6:7992
53. Wang XR, Liu JY, Liu ZW, Wang WC, Luo J, Han XP, Du XW, Qiao SZ, Jing Y (2018) Identifying the key role of pyridinic-N-Co bonding in synergistic electrocatalysis for reversible ORR/OER. Adv Mater 30:1870164
54. Zhang J, Zheng C, Zhang M, Qiu Y, Xu Q, Cheong WC, Chen W, Zheng L, Gu L, Hu Z, Wang D, Li Y (2020) Controlling N-doping type in carbon to boost single-atom site Cu catalyzed transfer hydrogenation of quinoline. Nano Res 13:3082–3087
55. Liu C, Wu Y, Sun K, Fang J, Huang A, Pan Y, Cheong WC, Zhuang Z, Zhuang Z, Yuan Q, Xin HL, Zhang C, Zhang J, Xiao H, Chen C, Li Y (2021) Constructing FeN_4/graphitic nitrogen atomic interface for high-efficiency electrochemical CO_2 reduction over a broad potential window. Chem 7:1–11

Authors and Affiliations

Jianbo Zhao[1] · Weichuang Yang[1] · Haifeng Yuan[1] · Xiaomeng Li[1] · Wanzhen Bing[1] · Lifeng Han[2] · Konglin Wu[3]

[1] School of Material and Chemical Engineering, Zhengzhou University of Light Industry, Zhengzhou 450001, People's Republic of China

[2] Henan Provincial Key Laboratory of Surface and Interface Science, Zhengzhou University of Light Industry, Zhengzhou 450001, People's Republic of China

[3] Institute of Clean Energy and Advanced Nanocatalysis, School of Chemistry and Chemical Engineering, Anhui University of Technology, Maanshan 243002, People's Republic of China